HHS Public Access

Author manuscript

Cancer Lett. Author manuscript; available in PMC 2022 April 10.

Published in final edited form as:

Cancer Lett. 2021 October 10; 518: 59–71. doi:10.1016/j.canlet.2021.06.007.

Hedgehog Transcriptional Effector GLI Mediates mTOR-Induced PD-L1 Expression in Gastric Cancer Organoids

Vivien Koh[1,2,**], **Jayati Chakrabarti**[3,**], **Meaghan Torvund**[3], **Nina Steele**[4], **Jennifer A. Hawkins**[5], **Yoshiaki Ito**[2], **Jiang Wang**[6], **Michael A. Helmrath**[5], **Juanita L. Merchant**[7], **Syed Ahmed**[8], **Asim Shabbir**[9], **Jimmy Bok Yan So**[1,10], **Wei Peng Yong**[1,2,*], **Yana Zavros**[3,*]

[1]National University Cancer Institute Singapore, National University Health System, Singapore

[2]Cancer Science Institute of Singapore, National University of Singapore

[3]Department of Cellular and Molecular Medicine, University of Arizona, Tucson, AZ, USA

[4]Department of Cell and Developmental Biology and Department of Surgery, University of Michigan, Ann Arbor MI, USA

[5]Department of Pediatric Surgery, Cincinnati Children's Hospital Medical Center, Cincinnati, OH, USA

[6]Department of Pathology and Laboratory Medicine, University of Cincinnati College of Medicine, Cincinnati, OH, USA

[7]Department of Gastroenterology and Hepatology, University of Arizona College of Medicine, Tucson AZ, USA

[8]Department of Surgery, University of Cincinnati Cancer Institute, Cincinnati, OH, USA

[9]Department of Surgery, National University Hospital, Singapore

[10]Department of Surgery, Yong Loo Lin School of Medicine, National University of Singapore

Abstract

Objective: Tumors evade immune surveillance by expressing Programmed Death-Ligand 1 (PD-L1), subsequently inhibiting CD8+ cytotoxic T lymphocyte function. Response of gastric cancer to immunotherapy is relatively low. Our laboratory has reported that *Helicobacter pylori*-induced PD-L1 expression within the gastric epithelium is mediated by the Hedgehog (Hh) signaling pathway. The PI3K/AKT/mTOR pathway is activated in gastric cancer and may have immunomodulatory potential. *We hypothesize that Hh signaling mediates mTOR-induced PD-L1 expression.*

Design: Patient-derived organoids (PDOs) were generated from gastric biopsies and resected tumor tissues. Autologous organoid/immune cell co-cultures were used to study the immunosuppressive function of MDSCs. NanoString Digital Spatial Profiling (DSP) of immune-

Correspondence: Yana Zavros PhD, Professor, Associate Head for Research, University of Arizona College of Medicine, Department of Cellular and Molecular Medicine; Yeoh Ghim Seng Visiting Professor, Department of Surgery, National University of Singapore, 1501 N Campbell Avenue, Life Sciences North Room 450, Tucson, AZ 85724, Tel: (520) 626-6084, yzavros@email.arizona.edu. *: Co-corresponding authors.

**:These authors contributed equally

related protein markers using FFPE slide-mounted tissues from gastric cancer patients was performed.

Results: DSP analysis showed infiltration of immunosuppressive MDSCs expressing Arg1, CD66b, VISTA and IDO1 within cancer tissues. Orthotopic transplantation of patient derived organoids (PDOs) resulted in the engraftment of organoids and the development of histology similar to that observed in the patient's tumor tissue. PDO/immune cell co-cultures revealed that PD-L1-expressing organoids were unresponsive to nivolumab *in vitro* in the presence of PMN-MDSCs. Depletion of PMN-MDSCs within these co-cultures sensitized the organoids to anti-PD-1/PD-L1-induced cancer cell death. Rapamycin decreased phosphorylated S6K, Gli2 and PD-L1 expression in PDO/immune cell co-cultures. Transcriptional regulation of PD-L1 by GLI1 and GLI2 was blocked by rapamycin.

Conclusions: The PDO/immune cell co-cultures may be used to to study immunosuppressive MDSC function within the gastric tumor microenvironment. The mTOR signaling pathway mediates GLI-induced PD-L1 expression in gastric cancer.

1. INTRODUCTION

Gastric cancer is the fifth most common cancer and the third leading cause of cancer-related mortality worldwide [1]. The 5-year survival rate varies in the range of 20-40% with a case fatality rate at approximately 70% because most gastric cancer patients are in the advanced stage at the time of diagnosis [2]. Treatment for advanced-stage gastric cancer primarily relies on combination chemotherapy [3]. However, outcomes are often hampered by severe side effects, hence better treatment is still required.

Early observations from our laboratory demonstrated that CagA stimulates Sonic Hedgehog (Shh) signaling within parietal cells, a response that is mediated by NFkB signaling [4, 5]. We then showed that the gastric morphogen, Shh, is fundamental to the initiation of gastritis in response to *H. pylori* infection [4]. Following these studies, we used iPSC- and tissue-derived human gastric organoid cultures to report that *H. pylori*-induced immune checkpoint molecule programmed cell death 1 ligand (PD-L1), is mediated by Hedgehog (Hh) signaling [6]. In these studies, PD-L1 was localized to Spasmolytic Polypeptide (TFF2)-Expressing Metaplastic (SPEM) cells as a mechanism by which these cells may survive chronic inflammation, for the persistence of infection and progression of disease to cancer [6]. In gastric cancer, Hh signaling mediates PD-L1 expression within tumor cells [7], but, the exact mechanism is unclear. In gastric cancer, the mechanistic target of rapamycin (mTOR) is often deregulated and has been validated as one of the therapeutic targets [8]. Many mTOR inhibitors have been developed and more mTOR inhibitors are being evaluated in clinical trials. Clinical data have demonstrated that mTOR inhibitors, in combination with standard chemotherapy or immunotherapy, serve as effective targeted cancer therapeutics for gastric cancer [9]. Of relevance to the studies here, activation of the AKT/mTOR pathway plays a role in the regulation of PD-L1 [10], the pathogenesis of *H. pylori* [11] and the regulation of metaplasia [12]. In esophageal adenocarcinoma, there is an established a crosstalk between the mTOR/S6K1 and the Hh pathway, via smoothened-independent Gli1 activation, and provides a rationale for combination therapy [13]. Thus, here we hypothesize that mTOR may regulate PD-L1 via a non-canonical, smoothened-independent Hh pathway.

The application of checkpoint blockade immunotherapy has shown promise in several solid tumors, including gastric adenocarcinomas [14-16]. Although antibodies that inhibit programmed cell death 1 (PD-1) and programmed death-ligand 1 (PD-L1) have emerged as promising immunotherapy for patients with gastric cancer, only a subset of patients have benefitted from them and most of them who initially responded will eventually develop acquired resistance [17-20]. There are currently no established selection criteria to predict whether a patient will benefit from immunotherapy alone or with combination therapy. Multiple suppressive immune cell types including macrophages, myeloid derived suppressor cells (MDSCs) and regulatory T cells (Tregs) accumulate within the tumor microenvironment (TME) of different malignancies. Of relevance to the studies presented here, MDSCs are known to block CD8+ cytotoxic T cell anti-tumor activity through L-arginine and L-cysteine sequestration as well as production of reactive oxygen species (ROS) [21] [22] [23]. Increased MDSC infiltration in the gastric cancer correlates with more advanced gastric cancer and reduced survival [24, 25]. Thus, the depletion of MDSCs to impair tumor growth may be proposed as an anti-cancer therapeutic strategy [26]. However, methods to deplete MDSCs in gastric cancer are currently largely unknown.

One of the greatest advancements in cell culture technologies over the past decade is the development of three-dimensional organoids as *in vitro* models for drug screening and cancer therapeutics [27-30]. Patient-derived organoids (PDOs) have been described for various tissues, but there are at present no gastric cancer PDOs that can be exploited as a high-fidelity preclinical model to predict the efficacy of immune checkpoint inhibition or elucidate the related molecular mechanisms of cancer immunology *in vitro*. In this study, we report the generation of an autologous cancer PDO/immune cell co-culture system that may be used to investigate PD-L1/PD-1 blockade together with the inhibition of immunosuppressive cells MDSCs for the development of therapeutic approaches for the treatment of gastric cancer.

2. MATERIALS AND METHODS

Patient selection and study population

All patients underwent total or subtotal gastrectomy at the National University Hospital of Singapore. Patients were eligible for study enrollment if they had a histologically or cytologically confirmed diagnosis of primary gastric cancer, were 21 years or older, and had never undergone prior chemotherapy or radiotherapy. Patients were ineligible if they had symptomatic or progressive central nervous system metastases, or other uncontrolled medical disorders. Study protocols were reviewed and approved by the National Healthcare Group Domain Specific Review Board (NHG DSRB; Reference Numbers: 2005/00440, 2016/00059) and complied with local laws and regulations. All patients provided written informed consent before study enrolment. The study was conducted in accordance with the Declaration of Helsinki and International Conference on Harmonisation and Good Clinical Practice guidelines. Tumor tissue was also obtained from patients undergoing surgical resection for gastric cancer (IRB protocol number: 2015-5537, University of Cincinnati; or IRB protocol number: 1912208231R001, University of Arizona Human Subjects Protection Program; IRB protocol number: 1099985869R001, University of Arizona Human Subjects

Protection Program TARGHETS). Demographics and clinicopathological profiles of the patients are summarized in Supplemental Table 1.

Generation and maintenance of gastric PDOs

Human gastric tissues were biopsied from the tumour and matched adjacent normal sites of each patient during surgical procedure and processed as described previously [31, 32]. Briefly, tissues were first minced and washed in Dulbecco's phosphate-buffered saline (DPBS; Thermo Fisher Scientific, Waltham, MA), and then digested in DPBS containing 1 mg/ml collagenase (Sigma-Aldrich, Saint Louis, MI) and 2 mg/ml bovine serum albumin (BSA; Sigma-Aldrich) for 30 minutes at 37°C. Digested tissues were passed through 30 μm filters (Miltenyi Biotec, Bergisch Gladbach, Germany). Filtered cells were pelleted at 300 × *g* for 5 minutes, resuspended in Matrigel (Corning Life Sciences, Corning, NY), and seeded into multiwell plates (Thermo Fisher Scientific). Cultures were maintained in gastric PDOs culture medium (Supplementary Table 2) at 37°C in 5% CO_2 and monitored daily for organoid generation. The culture medium in each well was replaced with fresh medium on alternate days. PDOs were passaged once every 7-10 days in 1:3 ratio.

Isolation of peripheral blood mononuclear cells (PBMCs) from whole blood

Whole blood was collected from gastric cancer patients during surgical procedure. PBMCs were isolated using Ficoll-Paque density gradient medium (GE Healthcare, Chicago, IL) following manufacturer's instructions. Briefly, whole blood was first diluted with DPBS, overlaid onto Ficoll-Paque medium, and then centrifuged at 400 × *g* for 30 minutes without brake. After centrifugation, mononuclear cells at the interface were transferred to a new tube, diluted with DPBS, and pelleted at 400 × *g* for 10 minutes. Cells were washed once with DPBS and then used in downstream applications.

Isolation and maturation of human dendritic cells

Dendritic cells were isolated and matured from PBMCs as described previously [33]. Briefly, PBMCs were cultured in AIM V medium (Thermo Fisher Scientific) supplemented with 10% human serum AB (Gemini Bio-Products, West Sacramento, CA), 50 μM β-mercaptoethanol (Thermo Fisher Scientific), 800 U/ml granulocyte-macrophage colony-stimulating factor (GM-CSF; Thermo Fisher Scientific) and 500 U/ml interleukin 4 (IL-4; Thermo Fisher Scientific) for 3 days. On day 3, the dendritic cell cultures were renewed with fresh medium additionally supplemented with 5 ng/ml tumor necrosis factor α (TNF-α; Thermo Fisher Scientific), 5 ng/ml interleukin 1β (IL-1β; Thermo Fisher Scientific), 150 ng/ml interleukin 6 (IL-6; Thermo Fisher Scientific) and 1 μg/ml prostaglandin E2 (PGE2; Thermo Fisher Scientific), and further maintained for 24 hours. Dendritic cells were then harvested for downstream applications.

Isolation and culture of human CTLs

Human CTLs were isolated from PBMCs using the EasySep Human CD8+ T Cell Enrichment Kit (STEMCELL Technologies, Vancouver, Canada) following manufacturer's instructions. Briefly, PBMCs were incubated with 50 μl/ml of Enrichment Cocktail for 10 minutes at room temperature. After which, 150 μl/ml of Magnetic Particles were added to

the sample and incubated for 5 minutes at room temperature. The sample was then diluted with EasySep Buffer (STEMCELL Technologies) and placed into an EasySep Magnet (STEMCELL Technologies) for cell separation. CTLs were recovered by transferring the cell suspension into a new tube and centrifuging at 300 × *g* for 5 minutes, and cultured in T cell medium as described previously.

Isolation and culture of human MDSCs

Human MDSCs were isolated from PBMCs as described previously [34]. Briefly, PBMCs were cultured in AIM V medium containing 50% conditioned medium collected from organoid cultures, 10 ng/ml IL-1β, 10 ng/ml IL-6, 1 μg/ml PGE2, 2 ng/ml transforming growth factor beta 1 (TGF-β1; Thermo Fisher Scientific), 10 ng/ml TNF-α, 10 ng/ml vascular endothelial growth factor (VEGF; Thermo Fisher Scientific) and 10 ng/ml GM-CSF for 7 days. MDSCs were then harvested for downstream applications.

Establishment of co-cultures of PDOs and immune cells

Co-cultures were established as described previously [7, 30]. Briefly, dendritic cells were first pulsed with conditioned medium collected from organoid cultures and then cultured with CTLs for 24 hours. CTLs were then collected and incubated with 5 μM carboxyfluorescein diacetate succinimidyl ester (CFSE; BioLegend, San Diego, CA) at 37°C for 20 minutes following manufacturer's instructions. CFSE is a blue laser excitable dye that can be used for flow cytometric monitoring of cell divisions. PDOs were harvested, mixed with CFSE-labelled CTLs, resuspended in an appropriate volume of Matrigel and seeded into multiwell plates. For experimental conditions requiring MDSCs, MDSCs were mixed with PDOs and CFSE-labelled CTLs, and seeded. Co-cultures were maintained in gastric PDOs culture medium at 37°C in 5% CO_2.

Drug treatment of PDO-immune cell co-cultures

The following groups of drug treatment conditions were established: 1) vehicle-treated PDOs, 2) vehicle-treated co-cultures of PDOs and CTLs, 3) co-cultures of PDOs and CTLs treated with 0.5 μg/ml nivolumab (anti-PD-1; Selleck Chemicals, Houston, TX) or 4) 10 μM cabozantinib (multiple receptor tyrosine kinases inhibitor; Sigma-Aldrich) alone, 5) co-cultures of PDOs, CTLs and MDSCs treated with 0.5 μg/ml nivolumab alone or 6) in combination with 10 μM cabozantinib. Cultures were treated for 48 hours and monitored using brightfield microscopy (Nikon Corporation, Tokyo, Japan).

Gene ChIP Assay

In order to investigate GLI-bound PD-l1 transcription factor, chromatin immunoprecipitation (ChIP) assays were performed using the Thermo Scientific™ Pierce™ Agarose ChIP kit following the manufacturer's protocol. Briefly, MSI-H cells were treated without/with GLI-inhibitor GANT61 (Stemcell technologies) for 48 hrs, fixed with formaldehyde to crosslink and preserve protein-DNA interactions. Protein-DNA complexes were sheared using Micrococcal Nuclease digestion, followed by immunoprecipitation with ChIP-grade antibodies against GLI1 (R&D AF3324), GLI2 (R&D AF3526), positive (anti-RNA polymerase II antibody) and negative (Normal Rabbit IgG) control used for protein-bound

DNA sequences. Crosslinking was reversed using NaCl and protein was digested using Proteinase K. GLI-bound PD-L1 expression were quantified using quantitative RT PCR with PD-L1 primer (Thermofisher Scientific).

Digital spatial profiling (DSP) of tissue microarrays (TMAs)

Commercial TMAs of normal stomach tissues and gastric cancer were purchased from Biochain (Newark,CA). Each TMA consists of 5 normal stomach or 50 tumour areas from formalin-fixed paraffin-embedded (FFPE) specimens arrayed on independent slides. Tissue specimens were used with approval from the Biochain Human Research Protections (OHRP registration number, IRB00008283) with an assurance filed with and approved by the United States Department of Health and Human Services. Approval includes informed consent or waiver of consent in accordance with the ethical guidelines of the United States Common Rule.

DSP was performed based on the nCounter barcoding technology (NanoString Technologies, Seattle, WA). Briefly, the FFPE TMAs were first deparaffinised and subjected to antigen retrieval procedures. The TMAs were then incubated overnight with three fluorescent-labelled visualisation antibodies and a cocktail of 40 unique primary antibodies [35] to detect epithelial, stromal and immune cell markers. After staining, the slides were scanned using the GeoMx DSP instrument (NanoString Technologies) to produce a digital fluorescent image of the tissues. Next, individual regions of interest (ROIs) covering the entire TMA core were generated and segmented into three molecularly-defined tissue compartments by fluorescent co-localisation: epithelium (tumour), non-immune cell stroma, and immune cell. Oligos from these compartments were released upon exposure to ultraviolet light in a sequential manner, collected by microcapillary aspiration, dispensed into a 96-well plate, hybridized to 4-colour 6-spot optical barcodes, and finally digitally counted in the nCounter system (NanoString Technologies). Digital counts from barcodes corresponding to protein probes were first normalised to internal spike-in controls (ERCCs) and then to the area of their compartment. Compartments with less than 10 nuclei or with an area of illumination (AOI) less than 100 μm^2 were excluded.

Histology and immunohistochemistry of PDOs

PDOs were harvested in intact Matrigel and transferred to 500 μl of molten HistoGel (Thermo Fisher Scientific) in a plastic cryomold (15 mm × 15 mm × 5 mm; Tissue-Tek, Sakura Finetek Europe, The Netherlands). The HistoGel was allowed to solidify on ice for 10 minutes, removed from the plastic cryomold, enclosed in a standard plastic cassette (Simport Scientific, Quebec, Canada), and fixed with 4% paraformaldehyde (Sigma-Aldrich) for 1 hour before embedding into paraffin blocks. PDO blocks were then sectioned and processed for haematoxylin and eosin (H&E; Merck Millipore, Burlington, MA) staining.

Immunohistochemistry was performed as described previously [29]. Briefly, tissues were fixed in 4% paraformaldehyde, embedded into paraffin blocks and sectioned at 5-μm thickness. After deparaffinization, antigen retrieval was performed by incubating the slides in 10 mM sodium citrate buffer at 100°C for 10 minutes. Endogenous peroxidase activity

was first blocked with 0.3% hydrogen peroxide for 10-15 minutes, followed by blocking of non-specific sites with 10% goat serum for 30 minutes. Sections were then incubated with anti-cytokeratin 7 (1:100; Novus Biologicals, Littleton, CO) or anti-PD-L1 (1:100; Novus Biologicals) at 4°C overnight. After which, sections were incubated with biotinylated anti-mouse or anti-rabbit secondary antibodies (Thermo Fisher Scientific) for 30 minutes, followed by an additional 30 minutes with VectaStain ABC reagent (Vector Laboratories, Burlingame, CA). DAB (3,3'-diaminobenzidine) Substrate Kit (Vector Laboratories) was used for color development and sections were counterstained with hematoxylin (Thermo Fisher Scientific), dehydrated and then mounted with Permount (Thermo Fisher Scientific).

Flow cytometry

PDO-immune cell co-cultures after 48 hours of treatment were incubated in Accutase (Innovative Cell Technologies, San Diego, CA) at 37°C for 15 minutes to dissociate PDOs into single cells. All cells were pelleted at 300 × *g* for 5 minutes, resuspended in 100 μl of 5% BSA, and stained with Zombie Red dye followed by fluorochrome-conjugated antibodies specific for human: CD8, CD14, CD15, CD33, CD11b, CD137, EpCAM, HLA-DR, and PD-L1 or mouse: CD8, Ly6C, Ly6G, CD11b, CD11C, EpCAM, BrdU, HLA-DR, and PD-L1 (all from BioLegend) at 4°C for 30 minutes. Cells were pelleted and treated with the Cytofix/Cytoperm Fixation/Permeabilization Solution (BD Biosciences, San Jose, CA) following manufacturer's instructions. Cells were then resuspended in 100 μl of 5% BSA, and stained with fluorochrome-conjugated antibodies specific for perforin (from BioLegend) at 4°C for 30 minutes. Prior to flow cytometric analysis, cells were washed twice and resuspended in 100 μl of 5% BSA. Samples were analysed on the LSRFortessa system (BD Biosciences). An unstained sample and single stained UltraComp beads (Thermofisher Scientific) was used as a control for gating. Data were processed using FlowJo software (BD Biosciences).

Whole-mount immunofluorescence

Whole-mount immunofluorescence staining of PDOs and co-cultures with immune cells was performed as described previously [29]. Briefly, cultures were established in chamber slides (Thermo Fisher Scientific) and first fixed with 3.7% formaldehyde (Sigma-Aldrich) at room temperature for 15 minutes and then permeabilised with 0.5% Triton X-100 (Sigma-Aldrich) at room temperature for 20 minutes. Blocking was done with 2% goat serum (Thermo Fisher Scientific) at room temperature for 1 hour. Samples were incubated with primary antibodies anti-CD8 and anti-PD-L1 (both from Novus Biologicals, Littleton, CO) at 4°C overnight, washed with 0.01% Triton X-100, and then incubated with Alexa Fluor secondary antibodies (Thermo Fisher Scientific) at room temperature for 1 hour. Nuclei were counterstained with DAPI (4′,6-diamidino-2-phenylindole; Sigma-Aldrich). Images were captured using Zeiss LSM 880 confocal microscope (Carl Zeiss AG, Oberkochen, Germany).

Western Blot analysis

Patient derived normal and tumor gastric tissues were homogenized in ice-cold phosphatase free lysis buffer (0.1M NaCl, 0.01M Tris.Cl, 0.001M EDTA, 0.01mM EDTA, 0.01mM DTT, 0.001M PMSF, protease and phosphatase inhibitor), centrifuged at 13,000 x g for 15min and the supernatant were used for western blot analysis. The MSI-H organoids were

harvested after the co-culture with immune cells using cold DPBS, and centrifuged in 400 x g for 5 mins. The EpCAM positive cells were isolated by magnetic bead isolation using CELLectin™ Biotin Binder kit and CD236 biotinylated antibody (Thermofisher Scientific) following manufacturer's protocol. The bead-bound EpCAM positive cells were resuspended in phosphatase free lysis buffer. The protein concentration was measured using Bradford kit (Thermofisher Scientific) and cell lysates were diluted in 4X Laemmli loading buffer containing β-mercaptoethanol (Bio-Rad Laboratories). Samples were loaded onto 4–20% Tris-Glycine Gradient Gels (Thermofisher Scientific) and run at 80 volts for approximately 3 hours and transferred to nitrocellulose membranes (Whatman Protran, 0.45 μM) at 105 volts for 1.5 hours at 4°C. Membranes were blocked for 1 hour at room temperature using KPL Detector Block Solution (Kirkegaard & Perry Laboratories, Inc). Membranes were incubated overnight at 4°C with either 1:1000 dilution of anti-AKT, anti-phospho AKT, anti-ERK, anti-phospho ERK, anti-S6K, anti-phospho S6K or 1:2000 dilution of mouse anti-GAPDH (Millipore, MAB374) antibodies followed by 1 hour incubation with a 1:1000 dilution anti-mouse, or -rabbit Alexa Fluor 680 (Thermofisher Scientific). Blots were imaged using a scanning densitometer along with analysis software (Odyssey Infrared Imaging Software System). All primary antibodies were purchased from Cell Signaling Technologies unless otherwise mentioned. Densitometric analysis was performed using the ImageJ - NIH.

Establishment of co-cultures of MSI-H gastric tumor spheroids and immune cells using AggreWell™ Microwell plates

To generate cell aggregates/spheroids, AggreWell™800 microwell plates, where each well contains an array of 300 microwells which are 800 μm in size, (Stemcell Technologies, 24 well) were used. The spheroids (MSI-H) were generated according to manufacturer's instruction. Concisely, 500ml Anti-adherence rinsing solution (Stemcell Technologies) was added to each well and centrifuged at 1300 x g for 5 minutes in a swinging bucket rotor, rinsed with warm 2ml basal medium/well and 1 ml complete medium was added to each well. The full-grown MSI-H gastric tumor derived organoids were harvested in cold DPBS and centrifuged at 400 x g, 5 min. The pellet was incubated with Accutase, at 37°C for 12 min, syringed (26G needle) gently 10 times. One mL complete growth media was added to the tube and centrifuged at 400 x g, 5 min. The cells were resuspended in complete media, added to each well (1ml/well), pipette gently up and down several times to evenly distribute the cells throughout the well and immediately centrifuged the AggreWell™ plate at 100 x g for 3 minutes. This culture was maintained for 72 hrs and immune cells (CTLs and/or MDSCs) were added to appropriate wells and immediately the plate was centrifuged at 100 x g for 3 min. The co-culture was treated with either nivolumab or cabozantinib or in combination. The spheroid/immune cell co-culture were imaged for 24, 48 and 72 hrs using brightfield microscopy (Nikon Spinning disk confocal microscope). The changes in area for each experimental conditions per timepoint were measured using Nikon Element software by manually drawing ROIs around individual spheroids from each microwell. The summarized area ± SEM was calculated and plotted as histogram using Graphpad Prism software. Statistical significance was determined when $p < 0.05$.

Morphological Analysis

Organoids growing in AggreWell™800 plates were imaged using a Nikon Ti2 Eclipse inverted microscope with a Plan Fluor 10X/0.3 objective pre- treatment, 48 hours post-treatment, and 72 hours post-treatment. Image scaling was set using known μM/pixel measurements, and in-focus organoids were outlined using the ImageJ freehand tool to collect area measurements. Area was normalized to pre-treatment values for each condition and graphed using GraphPad Prism. Regions of interest (ROIs) were drawn manually around individual organoids and automated measurement of density/area calculated using the Nikon Element Software Version 5.21.02. Density/area was calculated based on squared perimeter (μM^2). The circularity was measured using the formula, 4x pi x (area/squared perimeter). The changes in Density were analyzed per area/squared perimeter. Determination of Nuclear Area Factor was based on the measurement of the nuclear area and circularity using image analysis software.

Orthotopic Transplants

Orthotopic transplantations of gastric organoids were performed in NSG mice. Briefly, an acetic acid injury was induced as previously described [32, 36, 37] and following injury, approximately 500 organoids were injected within the submucosa of the previously injured site according to our previously published protocol [32].

Statistical analyses

Significance of the results was tested by two-way ANOVA or Student's t-test using Prism (GraphPad Software, San Diego, CA). P-value <0.05 was considered as significant.

3. RESULTS

PD-L1 and PMN-MDSCs are expressed within the gastric cancer TME and inhibit CTL proliferation and effector function

NanoString Digital Spatial Profiling (DSP) of immune-related protein markers using FFPE slide-mounted tissues from gastric cancer patients and normal stomachs was performed. We selected 6-12 regions of interest (ROIs) in the tumor microenvironment (Fig. 1B) and in normal stomach (Fig. 1A). Expressions of immunosuppressive cell markers were significantly higher in FFPE gastric cancer patient tissues (Fig. 1C; ***p<0.001**), when compared to normal stomach controls. We also observed a significant increase in PD-L1 within the tumor (PanCK-positive) compartment of the tissues (Fig. 1D-F). Immunofluorescence demonstrated elevated expression of PD-L1 and phosphor-S6K (Fig. 1G-I), and immunoblot showed increased GLI2 and phospho-S6K expression (Fig. 1J, K) in gastric cancer tissues from individual patients.

To identify the mechanisms by which PMN-MDSCs regulate PD-L1 expression and CTL function within the gastric cancer TME, gastric cancer organoids were generated from either resected tumor tissues or biopsies. We have previously developed and reported an orthotopic transplantation model using the human-derived tumor gastric organoids (huTGOs) [29]. Normal gastric (huFGO) and the huTGO organoid lines were transplanted into the gastric epithelium of NSG mice. Supplemental Fig. 1 shows the comparison of H&E, cytokeratin 7

(CK7) and PD-L1 expression between the organoid line in comparison to the patient's tumor tissue from which these were derived, and an orthotopic transplant. These data suggest that transplantation of huTGOs engraft within the gastric epithelium and mimic their parental histology.

PMN-MDCSs disrupt the efficacy of checkpoint inhibition in mouse-derived organoid/immune cell co-culture

To investigate whether PMN-MDSCs disrupt the efficacy of checkpoint inhibition in gastric tumor survival, we developed a gastric cancer organoid/CTL/MDSC co-culture. Supplemental Fig. 2A is an overview of our experimental approach developed by the research team to co-culture gastric cancer organoids with autologous patient immune cells. Data were collected and analyzed within 10 days of the start of organoid and immune cell co-cultures (Supplemental Fig. 2A). Importantly, tumor antigen-pulsing of DCs and CTL activation at day 4 of the protocol are fundamental to attempt to develop an in vitro system that is closest to physiological relevance. Supplemental Fig. 2B is a representative immunofluorescence image of CD8-positive T cells within the gastric cancer organoid culture. Flow cytometric analysis was performed using dissociated single cells isolated from biopsy tissue, matched patient-derived gastric cancer organoids (PDO) and the co-culture (PDO+CTL+MDSC). The ratio of the percentage of EpCAM+PD-L1+, CD8+ and PMN-MDSCs was similar between the 3 groups (Supplemental Fig. 2C, D) demonstrating that the key cellular compartments relevant to the studies were closely recapitulated in *in vitro* cultures.

Autologous organoid/CTL co-cultures treated with nivolumab exhibited significant organoid death (condition 2, Fig. 2A, B, E) compared to untreated controls (condition 1, Fig. 2A, B, E). Importantly, when PMN-MDSCs were added to the co-culture, this response was inhibited (condition 4, Fig. 2A, B, E). Addition of cabozantinib (cabo) to the organoid/CTL/MDSC co-culture depleted MDSCs from the culture and maximized the efficacy of checkpoint inhibition to induce PD-L1 expressing cancer organoid death (condition 5, Fig. 2A, B, E). Organoid death was quantified by flow cytometry of Zombie (viability dye)+/EpCAM+/PD-L1+ cells. To identify the impact of PMN-MDSCs on CD8+ T cell proliferation, we next assayed cell CFSE uptake within the same co-culture. CD8+ T cells within cultures of gastric cancer organoids without PMN-MDSCs exhibited an increase in CTL proliferation in response to nivolumab (condition 2, Fig. 2C, D). This proliferative response was diminished with the introduction of PMN-MDSCs within the co-culture (condition 4, Fig. 2C, D). Interestingly, combinatorial treatment with nivolumab and cabozantinib, resulted in the induction of CD8+ T cell proliferation (condition 5, Fig. 2C, D) that correlated with the depletion of PMN-MDSCs within culture conditions 4 and 5 (Fig. 2F).

Figure 3A is a schematic diagram of the established co-culture systems where we either: 1) cultured organoids and immune cells within the Matrigel dome, or 2) using AggreWell™ Microwell plates consisting of a high-density array of pyramid-shaped microwells, uniform organoids were generated. The area and density of the organoids were measured at 0, 48 and 72 hours post-treatment (Fig. 3B). Decreased organoid density were observed in

conditions 4 and 6 and reflective of cell death in response to nivolumab or combinatorial cabozantinib plus nivolumab treatment (Fig. 3C). Determination of Nuclear Area Factor was based on the measurement of the nuclear area and circularity using image analysis software. We observed that decreased nuclear area factor was an early indicator of cell morphological changes occurring during apoptosis in conditions 4 (nivolumab treatment) and 6 (combinatorial nivolumab and cabozantinib treatments) (Fig. 3C, D) [38]. While organoid growth, as measured by area, continued over 72 hours in condition 1, 2, 3 and 5, cell growth was halted in response to nivolumab (condition 4) or combinatorial cabozantinib plus nivolumab treatment (condition 6) (Fig. 3E).

Co-cultures were established using the PD-L1-positive MSI-high IM95 gastric cancer cell line-derived organoids with HLA matched CTL and MDSC immune cells as a positive control for experiments using PD-L1-expressing PDOs. Treatment with nivolumab in the absence of MDSCs resulted in increased CTL proliferation and increased organoid death, as measured by percent positive Zombie+/EpCAM+/PD-L1+ cells and decreased organoid area (condition 2). These effects were abolished with the addition of MDSCs to the organoid/CTL co-culture environment (condition 4). Treatment of the MDSC-containing co-culture with nivolumab in conjunction with cabozantinib again induced CTL proliferation, resulting in organoid death (condition 5) (Fig. 4A, C, E). There was no response in experimental treatment groups 1-5 in co-cultures performed using normal gastric organoids (huFGOs) with patient-matched autologous CTL and MDSC immune cells (Fig. 4B, D, F). There was a significant decrease in the percentage of PMN-MDSCs detected in the MSI-H- and huFGO-derived/CTL/MDSC co-cultures (conditions 4 and 5, Fig. 4G, H). The resultant changes in organoid area of the organoid/immune cell co-cultures in MSI-H organoids (Fig. 4A) and normal huFGOs (Fig. 4B). These data reveal that in a gastric cancer cell line that highly expresses PD-L1 and known to respond to nivolumab treatment, the presence of PMN-MDSCs in culture suppresses CTL effector function which in turn inhibits cancer cell death.

MDSCs were differentiated and co-cultured with tumor antigen-pulsed DC-activated CTLs. We observed a decrease in CTL proliferation with increased number of immunosuppressive PMN-MDSCs (Supplemental Fig. 3A, B). In an additional experimental condition of vehicle-treated Control on PDO-immune cell co-cultures (PDO+CTL+MDSC) bright field micrographs demonstrated that while MDSCs have an immunosuppressive effect on CD8-positive cytotoxic T lymphocytes (Supplemental Figure 3B), in a co-culture with organoids there is no effect on the T cells due to the PD-L1/PD-1 interaction between the CTLs and tumor organoids (revised Supplemental Figure 3C). Using a flow cytometric-based CFSE T cell proliferation assay, we also observed that sunitinib (inhibitor of the STAT3 signaling pathway) decreased PMN-MDSC-mediated immunosuppression of CTLs almost as effectively as cabozantinib, whereasregorafenib (inhibitor of the MAPK signaling pathway) had no effect on PMN-MDSC-mediated suppression of CTL proliferation when compared to vehicle (Supplemental Fig. 3C, D). Collectively, these data demonstrate the differentiation of an immunosuppressive phenotype of PMN-MDSCs in the co-culture system. The immunosuppressive function of PMN-MDSCs can be targeted using cabozantinib.

Rapamycin sensitizes gastric cancer organoids to CTL-induced cell death and blocks the transcriptional regulation of PD-L1 by GLI

Organoid area, as a measurement of growth, continued to increase over 72 hours in conditions 1 (Fig. 5A), 2, (Fig. 5B), and 3 (Fig. 5C). Organoid growth was halted, or decreased, in response to nivolumab (condition 4, Fig. 5D) or rapamycin (condition 5, Fig. 5E) treatments alone. In conditions 6 (Fig. 5F) and 7 (Fig. 5G), the addition of MDSCs to the co-culture blocked organoid death in response to nivolumab and rapamycin treatments as indicated by increased area. However, combinatorial treatment with either cabozantinib plus nivolumab (condition 8, Fig. 5H), or cabozantinib plus rapamycin (condition 9, Fig. 5I) resulted in a significant decrease in organoid area as an indicator of increased organoid death over 72 hours. Co-culture conditions that exhibited decreased organoid area corelated with decreased density (Fig. 5J) and nuclear area factor (Fig. 5K). Co-culture conditions that exhibited decreased organoid area, as a reflection of increased cell death (conditions 4, 5, 8 and 9), correlated with reduced in PD-L1 expression (Fig. 5D, E, H, I).

Protein was extracted from magnetically isolated epithelial cells from the gastric cancer organoids and analyzed for phosphor-S6K and Gli2 expression by western blot (Fig. 6A, B). In co-culture conditions treated with rapamycin a significant decrease in phospho-S6K was observed (Fig.6A), and importantly this correlated with significantly reduced Gli2 expression (Fig. 6B). ChIP assay revealed that the transcriptional regulation of PD-L1 by Gli1 and Gli2 was blocked by both rapamycin and GANT61 treatment of cultures (Fig. 6C). Transcriptional regulation of PD-L1 by Gli1 and Gli2 was not inhibited in cultures treated with vismodegib (Fig. 6C). Collectively these data suggest that mTOR signaling pathway mediates Gli-induced PD-L1 expression in gastric cancer organoids.

4. DISCUSSION

Our analysis of the patient-derived gastric cancer organoid/immune cell co-cultures revealed the differentiation and polarization of the patient's MDSCs to an immune cell population expressing $CD33^{+}CD11b^{+}CD15^{+}CD14^{-}$. In humans two distinct subset of MDSCs exist, monocytic-MDSCs (M-MDSCs) and polymorphonuclear (or granulocytic)-MDSCs (PMN-MDSCs) [22] [23]. Infiltration of MDSCs within the gastric epithelium occurs early in response to a major risk factor of gastric cancer *Helicobacter pylori* (*H. pylori*). Following a sustained increase in the morphogen Sonic Hedgehog secretion and signaling, tumor associated macrophages and PMN-MDSCs are recruited to the infection site [4] [39, 40]. Recent characterization of the infiltrating PMN-MDSCs in response to *H. pylori* infection showed that these immunosuppressive cells express the myeloid differentiation factor, Schlafen (SLFN) family of proteins, a transcriptional target of GLI1, and the endogenous small, non-coding microRNA, miR130b [39, 40]. $SLFN4^{+}$ myeloid cells express VEGF, IL-1β and TNF-α, all known factors associated with MDSC regulation and represent an immunosuppressive cell of relevance to immunotherapy-resistant gastric cancer [39, 40]. We propose that these unique PMN-MDSCs may be sustained within the gastric TME. We demonstrated by DSP analysis of tissues sections collected from gastric cancer patients that there was a significant infiltration of CD68-positive monocyte cells that highly expressed arginase 1 (ARG1), CD66b, V-domain Ig suppressor of T-cell activation (VISTA) and

indoleamine 2,3-dioxygease (IDO1). The protein expression pattern of these CD68-positive monocytic cells was consistent with the PMN-MDSC phenotype. In support of our findings, MDSCs are known to utilize a number of mechanisms to suppress anti-tumor immunity. Such mechanisms include the expression of high levels of ARG1, iNOS or ROS, as well as the production of IDO1 [41-43]. In addition, evidence from acute myeloid leukemia (AML) demonstrates a strong positive association between MDSC expression of VISTA and T cell expression of PD-1 [44]. Increased MDSC infiltration in gastric cancer correlates with advanced stage and reduced survival [24, 25]. Thus, the depletion of MDSCs to impair tumor growth may be proposed for combination targeted therapy of gastric cancer [26] (Fig. 6D).

PMN-MDSCs play a functional role in the suppression of CTL effector function within the gastric cancer TME but also during *H. pylori* infection [39, 40]. Combinatorial therapy targeting the depletion of MDSCs with immunotherapy to enhance anti-tumor immunity has been tested in malignancies including melanoma, head and neck squamous cell carcinoma and prostate cancer patients [45] [46]. However, preclinical studies that evaluate the efficacy of targeting MDSCs in combination with chemotherapy and immunotherapy have not been previously reported in gastric cancer. This led us to the development of a PDO/immune cell co-culture system that may be used to identify such targeted MDSC disruption (Fig. 6D). Our *in vitro* data demonstrate that depleting PMN-MDSCs from the co-cultures using cabozantinib results in sensitization of the efficacy of nivolumab and increased CTL proliferation and effector function. Evidence from prostate, renal and breast cancer research, as well as clinical trials, has clearly documented that tyrosine kinase inhibitors (such as cabozantinib and sunitinib) target MDSC function or generation [47-49]. Cabozantinib-targeted MDSC depletion used in combination with immune checkpoint blockade induces anti-tumor activities and tumor regression in castration-resistant prostate cancer [49]. Based on the literature we postulated that cabozantinib, a tyrosine kinase inhibitor, targets MET, VEGFR2, FLT3, c-KIT and RET [50]. Phosphorylation of tyrosine residues on these receptors leads to the activation of downstream signaling pathways including MET, VEGFR2 and Jak/Stat [51], signaling pathways that are known to be expressed and activated in the presence of functional immunosuppressive MDSCs.

Our findings demonstrate that inhibition of mTOR by rapamycin increases immune cell effector function and that GLI-induced PD-L1 expression in gastric cancer organoids. In addition, we show the transcriptional regulation of PD-L1 by Gli1 and Gli2, a response mediated by mTOR signaling. Beyond its regulatory effects on immune cells, mTOR also regulates the expression of PD-L1 in cancer cells [52, 53]. We extend existing knowledge, using the gastric cancer organoid/immune cell co-cultures, that the mTOR pathway mediates Hedgehog signaling cascade to induce PD-L1 expression that is independent of smoothened (Fig. 6D). Hyperactivation of the mTOR pathway contributes significantly to tumorigenesis and malignancy, and targeting of the mTOR pathway is a potential cancer therapy strategy [54]. According to preclinical and clinical data, apart from attenuation of tumor development and metastasis, the therapeutic targeting of mTOR also enhances immunological surveillance and anti-tumor adaptive immune responses. Deregulation of mTOR signaling has been found to play crucial roles in regulating immune responses, such as T cell activation and myeloid cell differentiation [55]. Therefore, the mTOR

signaling pathway may be targeted to decrease PD-L1 expression and thus residence to immunotherapy and in gastric cancer cells. Nivolumab has demonstrated efficacious activity in chemotherapy-refractory gastric cancer and has recently been approved by the Food and Drug Administration (FDA) for frontline treatment of gastric cancer based on positive results from the CheckMate 649 study (NCT02872116) [56] [57, 58]. There are currently more than 50 clinical trials related to the enhanced efficacy of nivolumab either in combination with cabozantinib (36 studies) or sunitinib (16 studies) in several solid tumors, including melanoma, renal cell carcinoma and hepatocellular carcinoma [https://www.clinicaltrials.gov/]. Here, in our present study, we have demonstrated that nivolumab resistance mediated by MDSCs in gastric cancer organoid/immune cell co-cultures can be abolished by co-treatment with cabozantinib or sunitinib, further supporting clinical validation that has future therapeutic implication for gastric cancer patients.

Supplementary Material

Refer to Web version on PubMed Central for supplementary material.

Acknowledgements

This research is supported by: Singapore Ministry of Health National Medical Research Council under its Open Fund-Large Collaborative Grant (OF-LCG; MOH-OFLCG18May-0003) awarded to the Singapore Gastric Cancer Consortium; NIH (NIDDK) 2 R01 DK083402-06A1 grant, NIH 1U19AI116491-01 grant and Yeoh Ghim Seng Visiting Professorship in Surgery research fund from the National University of Singapore awarded to YZ; National Cancer Institute Singapore Centre Grant Programme awarded to WPY. This project was also supported in part by PHS Grant P30 DK078392 (Integrative Morphology Core) of the Digestive Diseases Research Core Center in Cincinnati. We are sincerely grateful to Jocelyn Fimbres in the Tissue Acquisition and Cellular/Molecular Analysis Shared Resource (TACMASR) Core for their assistance with embedding, sectioning and immunohistochemistry of tissue and organoids. We would also like to acknowledge Patty Jansma (Marley Imaging Core, University Arizona) and, Douglas W Cromey (TACMASR core, University of Arizona) for assistance in microscopy. Research reported also partly supported by the National Cancer Institute of the National Institutes of Health under award number P30 CA023074 (Sweasy). Merchant (R01 DK 118563). We would like to thank Dr. CHAN Shing Leng from the Cancer Science Institute of Singapore for her advice on organoid generation and critically reviewing the manuscript. We would also like to thank Fiona CHIA from the Microscopy Core Facility at the Cancer Science Institute of Singapore for her assistance with confocal microscopy, Chet Closson (Live Microscopy Core, University of Cincinnati and Lisa McMILLIN from the Pathology Research Core at Cincinnati Children's Hospital Medical Center for her assistance with histology.

REFERENCES

[1]. Bray F, Ferlay J, Soerjomataram I, Siegel RL, Torre LA, Jemal A, Global cancer statistics 2018: GLOBOCAN estimates of incidence and mortality worldwide for 36 cancers in 185 countries, CA Cancer J Clin, 68 (2018) 394–424. [PubMed: 30207593]

[2]. Allemani C, Matsuda T, Di Carlo V, Harewood R, Matz M, Niksic M, Bonaventure A, Valkov M, Johnson CJ, Esteve J, Ogunbiyi OJ, Azevedo ESG, Chen WQ, Eser S, Engholm G, Stiller CA, Monnereau A, Woods RR, Visser O, Lim GH, Aitken J, Weir HK, Coleman MP, Group CW, Global surveillance of trends in cancer survival 2000-14 (CONCORD-3): analysis of individual records for 37 513 025 patients diagnosed with one of 18 cancers from 322 population-based registries in 71 countries, Lancet, 391 (2018) 1023–1075. [PubMed: 29395269]

[3]. Wagner AD, Syn NL, Moehler M, Grothe W, Yong WP, Tai BC, Ho J, Unverzagt S, Chemotherapy for advanced gastric cancer, Cochrane Database Syst Rev, 8 (2017) CD004064. [PubMed: 28850174]

[4]. Schumacher MA, Donnelly JM, Engevik AC, Xiao C, Yang L, Kenny S, Varro A, Hollande F, Samuelson LC, Zavros Y, Gastric Sonic Hedgehog Acts as a Macrophage Chemoattractant During the Immune Response to Helicobacter pylori, Gastroenterology, 142 (2012) 1150–1159. [PubMed: 22285806]

[5]. Schumacher MA, Feng R, Aihara E, Engevik AC, Montrose MH, Ottemann KM, Zavros Y, Helicobacter pylori-induced Sonic Hedgehog expression is regulated by NFkappaB pathway activation: the use of a novel in vitro model to study epithelial response to infection, Helicobacter, 20 (2015) 19–28. [PubMed: 25495001]

[6]. Holokai L, Chakrabarti J, Broda T, Chang J, Hawkins JA, Sundaram N, Wroblewski LE, Peek RM Jr., Wang J, Helmrath M, Wells JM, Zavros Y, Increased Programmed Death-Ligand 1 is an Early Epithelial Cell Response to Helicobacter pylori Infection, PLoS Pathog, 15 (2019) e1007468. [PubMed: 30703170]

[7]. Chakrabarti J, Holokai L, Syu L, Steele NG, Chang J, Wang J, Ahmed S, Dlugosz A, Zavros Y, Hedgehog signaling induces PD-L1 expression and tumor cell proliferation in gastric cancer, Oncotarget, 9 (2018) 37439–37457. [PubMed: 30647844]

[8]. Fattahi S, Amjadi-Moheb F, Tabaripour R, Ashrafi GH, Akhavan-Niaki H, PI3K/AKT/mTOR signaling in gastric cancer: Epigenetics and beyond, Life Sci, 262 (2020) 118513. [PubMed: 33011222]

[9]. Bu Z, Ji J, Therapeutic implications of mTOR inhibitors in the treatment of gastric cancer, Curr Cancer Drug Targets, 13 (2013) 121–125. [PubMed: 23215721]

[10]. Lastwika KJ, Wilson W 3rd, Li QK, Norris J, Xu H, Ghazarian SR, Kitagawa H, Kawabata S, Taube JM, Yao S, Liu LN, Gills JJ, Dennis PA, Control of PD-L1 Expression by Oncogenic Activation of the AKT-mTOR Pathway in Non-Small Cell Lung Cancer, Cancer Res, 76 (2016) 227–238. [PubMed: 26637667]

[11]. Badary DM, Rahma M, Ashmawy AM, Hafez MZ, H. pylori infection increases gastric mucosal COX2 and mTOR expression in chronic gastritis: Implications for cancer progression?, Pathophysiology, 24 (2017) 205–211. [PubMed: 28668512]

[12]. Willet SG, Lewis MA, Miao ZF, Liu D, Radyk MD, Cunningham RL, Burclaff J, Sibbel G, Lo HG, Blanc V, Davidson NO, Wang ZN, Mills JC, Regenerative proliferation of differentiated cells by mTORC1-dependent paligenosis, EMBO J, 37 (2018).

[13]. Wang Y, Ding Q, Yen CJ, Xia W, Izzo JG, Lang JY, Li CW, Hsu JL, Miller SA, Wang X, Lee DF, Hsu JM, Huo L, Labaff AM, Liu D, Huang TH, Lai CC, Tsai FJ, Chang WC, Chen CH, Wu TT, Buttar NS, Wang KK, Wu Y, Wang H, Ajani J, Hung MC, The crosstalk of mTOR/S6K1 and Hedgehog pathways, Cancer Cell, 21 (2012) 374–387. [PubMed: 22439934]

[14]. Topalian SL, Taube JM, Pardoll DM, Neoadjuvant checkpoint blockade for cancer immunotherapy, Science, 367 (2020).

[15]. Demaria O, Cornen S, Daeron M, Morel Y, Medzhitov R, Vivier E, Harnessing innate immunity in cancer therapy, Nature, 574 (2019) 45–56. [PubMed: 31578484]

[16]. Demaria S, Romano E, Brackstone M, Formenti SC, Immune induction strategies to enhance responses to PD-1 blockade: lessons from the TONIC trial, J Immunother Cancer, 7 (2019) 318. [PubMed: 31752991]

[17]. Fuchs CS, Doi T, Jang RW, Muro K, Satoh T, Machado M, Sun W, Jalal SI, Shah MA, Metges JP, Garrido M, Golan T, Mandala M, Wainberg ZA, Catenacci DV, Ohtsu A, Shitara K, Geva R, Bleeker J, Ko AH, Ku G, Philip P, Enzinger PC, Bang YJ, Levitan D, Wang J, Rosales M, Dalal RP, Yoon HH, Safety and Efficacy of Pembrolizumab Monotherapy in Patients With Previously Treated Advanced Gastric and Gastroesophageal Junction Cancer: Phase 2 Clinical KEYNOTE-059 Trial, JAMA Oncol, 4 (2018) e180013. [PubMed: 29543932]

[18]. Bang YJ, Van Cutsem E, Fuchs CS, Ohtsu A, Tabernero J, Ilson DH, Hyung WJ, Strong VE, Goetze TO, Yoshikawa T, Tang LH, Hwang PMT, Webb N, Adelberg D, Shitara K, KEYNOTE-585: Phase III study of perioperative chemotherapy with or without pembrolizumab for gastric cancer, Future Oncol, 15 (2019) 943–952. [PubMed: 30777447]

[19]. Kawazoe A, Yamaguchi K, Yasui H, Negoro Y, Azuma M, Amagai K, Hara H, Baba H, Tsuda M, Hosaka H, Kawakami H, Oshima T, Omuro Y, Machida N, Esaki T, Yoshida K, Nishina T, Komatsu Y, Han SR, Shiratori S, Shitara K, Safety and efficacy of pembrolizumab in combination with S-1 plus oxaliplatin as a first-line treatment in patients with advanced gastric/gastroesophageal junction cancer: Cohort 1 data from the KEYNOTE-659 phase IIb study, Eur J Cancer, 129 (2020) 97–106. [PubMed: 32145474]

[20]. Smyth E, Knodler M, Giraut A, Mauer M, Nilsson M, Van Grieken N, Wagner AD, Moehler M, Lordick F, VESTIGE: Adjuvant Immunotherapy in Patients With Resected Esophageal,

Gastroesophageal Junction and Gastric Cancer Following Preoperative Chemotherapy With High Risk for Recurrence (N+ and/or R1): An Open Label Randomized Controlled Phase-2-Study, Front Oncol, 9 (2019) 1320. [PubMed: 32083013]

[21]. Zhang Y, Velez-Delgado A, Mathew E, Li D, Mendez FM, Flannagan K, Rhim AD, Simeone DM, Beatty GL, Pasca di Magliano M, Myeloid cells are required for PD-1/PD-L1 checkpoint activation and the establishment of an immunosuppressive environment in pancreatic cancer, Gut, 66 (2017) 124–136. [PubMed: 27402485]

[22]. Schouppe E, Van Overmeire E, Laoui D, Keirsse J, Van Ginderachter JA, Modulation of CD8(+) T-cell activation events by monocytic and granulocytic myeloid-derived suppressor cells, Immunobiology, 218 (2013) 1385–1391. [PubMed: 23932436]

[23]. Youn JI, Nagaraj S, Collazo M, Gabrilovich DI, Subsets of myeloid-derived suppressor cells in tumor-bearing mice, J Immunol, 181 (2008) 5791–5802. [PubMed: 18832739]

[24]. Wang L, Chang EW, Wong SC, Ong SM, Chong DQ, Ling KL, Increased myeloid-derived suppressor cells in gastric cancer correlate with cancer stage and plasma S100A8/A9 proinflammatory proteins, J Immunol, 190 (2013) 794–804. [PubMed: 23248262]

[25]. Wang PF, Song SY, Wang TJ, Ji WJ, Li SW, Liu N, Yan CX, Prognostic role of pretreatment circulating MDSCs in patients with solid malignancies: A meta-analysis of 40 studies, Oncoimmunology, 7 (2018) e1494113. [PubMed: 30288362]

[26]. Wesolowski R, Markowitz J, Carson WE 3rd, Myeloid derived suppressor cells - a new therapeutic target in the treatment of cancer, J Immunother Cancer, 1 (2013) 10. [PubMed: 24829747]

[27]. Drost J, Clevers H, Organoids in cancer research, Nat Rev Cancer, 18 (2018) 407–418. [PubMed: 29692415]

[28]. Dedhia PH, Bertaux-Skeirik N, Zavros Y, Spence JR, Organoid Models of Human Gastrointestinal Development and Disease, Gastroenterology, 150 (2016) 1098–1112. [PubMed: 26774180]

[29]. Steele NG, Chakrabarti J, Wang J, Biesiada J, Holokai L, Chang J, Nowacki LM, Hawkins J, Mahe M, Sundaram N, Shroyer N, Medvedovic M, Helmrath M, Ahmad S, Zavros Y, An Organoid-Based Preclinical Model of Human Gastric Cancer, Cell Mol Gastroenterol Hepatol, 7 (2019) 161–184. [PubMed: 30522949]

[30]. Chakrabarti J, Holokai L, Syu L, Steele N, Chang J, Dlugosz A, Zavros Y, Mouse-Derived Gastric Organoid and Immune Cell Co-culture for the Study of the Tumor Microenvironment, Methods Mol Biol, 1817 (2018) 157–168. [PubMed: 29959712]

[31]. Bertaux-Skeirik N, Feng R, Schumacher MA, Li J, Mahe MM, Engevik AC, Javier JE, Peek RM Jr., Ottemann K, Orian-Rousseau V, Boivin GP, Helmrath MA, Zavros Y, CD44 plays a functional role in Helicobacter pylori-induced epithelial cell proliferation, PLoS Pathog, 11 (2015) e1004663. [PubMed: 25658601]

[32]. Engevik AC, Feng R, Choi E, White S, Bertaux-Skeirik N, Li J, Mahe MM, Aihara E, Yang L, DiPasquale B, Oh S, Engevik KA, Giraud AS, Montrose MH, Medvedovic M, Helmrath MA, Goldenring JR, Zavros Y, The Development of Spasmolytic Polypeptide/TFF2-Expressing Metaplasia (SPEM) During Gastric Repair Is Absent in the Aged Stomach, Cell Mol Gastroenterol Hepatol, 2 (2016) 605–624. [PubMed: 27990460]

[33]. Nair S, Archer GE, Tedder TF, Isolation and generation of human dendritic cells, Curr Protoc Immunol, Chapter 7 (2012) Unit7.32.

[34]. Lechner MG, Liebertz DJ, Epstein AL, Characterization of cytokine-induced myeloid-derived suppressor cells from normal human peripheral blood mononuclear cells, J Immunol, 185 (2010) 2273–2284. [PubMed: 20644162]

[35]. Toki MI, Merritt CR, Wong PF, Smithy JW, Kluger HM, Syrigos KN, Ong GT, Warren SE, Beechem JM, Rimm DL, High-Plex Predictive Marker Discovery for Melanoma Immunotherapy-Treated Patients Using Digital Spatial Profiling, Clin Cancer Res, 25 (2019) 5503–5512. [PubMed: 31189645]

[36]. Engevik AC, Feng R, Yang L, Y. Z, The Acid-secreting parietal cell as an endocrine source of sonic hedgehog during gastric repair., Endocrinology, 154 (2013) 4627–4639. [PubMed: 24092639]

[37]. Xiao C, Feng R, Engevik A, Martin J, Tritschler J, Schumacher M, Koncar R, Roland J, Nam K, Goldenring J, Zavros Y, Sonic Hedgehog contributes to gastric mucosal restitution after injury., Lab Invest, 93 (2013) 96–111. [PubMed: 23090636]

[38]. Daniel B, DeCoster MA, Quantification of sPLA2-induced early and late apoptosis changes in neuronal cell cultures using combined TUNEL and DAPI staining, Brain Res Brain Res Protoc, 13 (2004) 144–150. [PubMed: 15296851]

[39]. Ding L, Hayes MM, Photenhauer A, Eaton KA, Li Q, Ocadiz-Ruiz R, Merchant JL, Schlafen 4-expressing myeloid-derived suppressor cells are induced during murine gastric metaplasia, J Clin Invest, 126 (2016) 2867–2880. [PubMed: 27427984]

[40]. Ding L, Li Q, Chakrabarti J, Munoz A, Faure-Kumar E, Ocadiz-Ruiz R, Razumilava N, Zhang G, Hayes MH, Sontz RA, Mendoza ZE, Mahurkar S, Greenson JK, Perez-Perez G, Hanh NTH, Zavros Y, Samuelson LC, Iliopoulos D, Merchant JL, MiR130b from Schlafen4(+) MDSCs stimulates epithelial proliferation and correlates with preneoplastic changes prior to gastric cancer, Gut, (2020).

[41]. Poschke I, Mougiakakos D, Hansson J, Masucci GV, Kiessling R, Immature immunosuppressive CD14+HLA-DR-/low cells in melanoma patients are Stat3hi and overexpress CD80, CD83, and DC-sign, Cancer Res, 70 (2010) 4335–4345. [PubMed: 20484028]

[42]. Corzo CA, Cotter MJ, Cheng P, Cheng F, Kusmartsev S, Sotomayor E, Padhya T, McCaffrey TV, McCaffrey JC, Gabrilovich DI, Mechanism regulating reactive oxygen species in tumor-induced myeloid-derived suppressor cells, J Immunol, 182 (2009) 5693–5701. [PubMed: 19380816]

[43]. Mougiakakos D, Jitschin R, von Bahr L, Poschke I, Gary R, Sundberg B, Gerbitz A, Ljungman P, Le Blanc K, Immunosuppressive CD14+HLA-DRlow/neg IDO+ myeloid cells in patients following allogeneic hematopoietic stem cell transplantation, Leukemia, 27 (2013) 377–388. [PubMed: 22828446]

[44]. Wang L, Jia B, Claxton DF, Ehmann WC, Rybka WB, Mineishi S, Naik S, Khawaja MR, Sivik J, Han J, Hohl RJ, Zheng H, VISTA is highly expressed on MDSCs and mediates an inhibition of T cell response in patients with AML, Oncoimmunology, 7 (2018) e1469594. [PubMed: 30228937]

[45]. Draghiciu O, Lubbers J, Nijman HW, Daemen T, Myeloid derived suppressor cells-An overview of combat strategies to increase immunotherapy efficacy, Oncoimmunology, 4 (2015) e954829. [PubMed: 25949858]

[46]. Mei Z, Huang J, Qiao B, Lam AK, Immune checkpoint pathways in immunotherapy for head and neck squamous cell carcinoma, Int J Oral Sci, 12 (2020) 16. [PubMed: 32461587]

[47]. Ko JS, Zea AH, Rini BI, Ireland JL, Elson P, Cohen P, Golshayan A, Rayman PA, Wood L, Garcia J, Dreicer R, Bukowski R, Finke JH, Sunitinib mediates reversal of myeloid-derived suppressor cell accumulation in renal cell carcinoma patients, Clin Cancer Res, 15 (2009) 2148–2157. [PubMed: 19276286]

[48]. Kodera Y, Katanasaka Y, Kitamura Y, Tsuda H, Nishio K, Tamura T, Koizumi F, Sunitinib inhibits lymphatic endothelial cell functions and lymph node metastasis in a breast cancer model through inhibition of vascular endothelial growth factor receptor 3, Breast Cancer Res, 13 (2011) R66. [PubMed: 21693010]

[49]. Lu X, Horner JW, Paul E, Shang X, Troncoso P, Deng P, Jiang S, Chang Q, Spring DJ, Sharma P, Zebala JA, Maeda DY, Wang YA, DePinho RA, Effective combinatorial immunotherapy for castration-resistant prostate cancer, Nature, 543 (2017) 728–732. [PubMed: 28321130]

[50]. Grullich C, Cabozantinib: a MET, RET, and VEGFR2 tyrosine kinase inhibitor, Recent Results Cancer Res, 201 (2014) 207–214. [PubMed: 24756794]

[51]. Trikha P, Carson WE 3rd, Signaling pathways involved in MDSC regulation, Biochim Biophys Acta, 1846 (2014) 55–65. [PubMed: 24727385]

[52]. Hua H, Kong Q, Zhang H, Wang J, Luo T, Jiang Y, Targeting mTOR for cancer therapy, J Hematol Oncol, 12 (2019) 71. [PubMed: 31277692]

[53]. Mossmann D, Park S, Hall MN, mTOR signalling and cellular metabolism are mutual determinants in cancer, Nat Rev Cancer, 18 (2018) 744–757. [PubMed: 30425336]

[54]. Guertin DA, Sabatini DM, Defining the role of mTOR in cancer, Cancer Cell, 12 (2007) 9–22. [PubMed: 17613433]

[55]. Weichhart T, Hengstschlager M, Linke M, Regulation of innate immune cell function by mTOR, Nat Rev Immunol, 15 (2015) 599–614. [PubMed: 26403194]

[56]. Kang YK, Boku N, Satoh T, Ryu MH, Chao Y, Kato K, Chung HC, Chen JS, Muro K, Kang WK, Yeh KH, Yoshikawa T, Oh SC, Bai LY, Tamura T, Lee KW, Hamamoto Y, Kim JG, Chin K, Oh DY, Minashi K, Cho JY, Tsuda M, Chen LT, Nivolumab in patients with advanced gastric or gastro-oesophageal junction cancer refractory to, or intolerant of, at least two previous chemotherapy regimens (ONO-4538-12, ATTRACTION-2): a randomised, double-blind, placebo-controlled, phase 3 trial, Lancet, 390 (2017) 2461–2471. [PubMed: 28993052]

[57]. Moehler M, Maderer A, Thuss-Patience PC, Brenner B, Meiler J, Ettrich TJ, Hofheinz RD, Al-Batran SE, Vogel A, Mueller L, Lutz MP, Lordick F, Alsina M, Borchert K, Greil R, Eisterer W, Schad A, Slotta-Huspenina J, Van Cutsem E, Lorenzen S, Cisplatin and 5-fluorouracil with or without epidermal growth factor receptor inhibition panitumumab for patients with non-resectable, advanced or metastatic oesophageal squamous cell cancer: a prospective, open-label, randomised phase III AIO/EORTC trial (POWER), Ann Oncol, 31 (2020) 228–235. [PubMed: 31959339]

[58]. N.p.c.v.c.a.f.-l.t.f.a.g.c.g.j.c.e.a.F.r.o.t.C. study., ESMO Virtual Congress, Annals of Oncology 31:S1142–S1215, (2020).

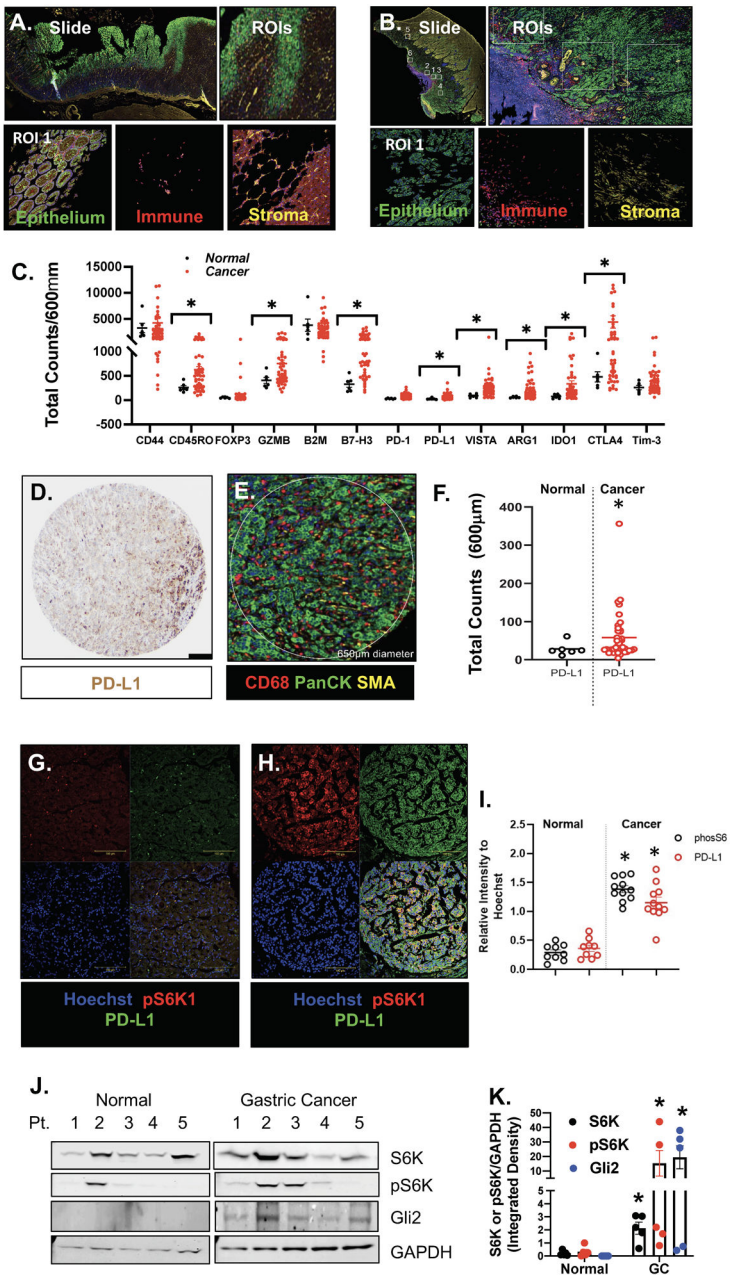

Figure 1: DSP analysis of FFPE tissues collected from normal and cancer gastric tissues.

Representative ROIs selected in **(A)** normal and **(B)** gastric cancer tissue. **(C)** Protein expression counts of immune (CD68+) cell markers in normal (black) and gastric cancer (red) tissues. **(D)** IHC staining showing expression of PD-L1 and **(E)** corresponding DSP ROI. **(F)** Protein expression counts of PD-L1 in PanCK+ normal (black) and gastric cancer (red) tissues. **(G, H)** Immunofluorescence using antibodies specific for the expression of PD-L1 (green) and phosphorylated S6K (pS6K1, red) in normal and cancer tissues. **(I)** Relative intensity of pS6K (black) and PD-L1 (red). **(J)** Western blots for the expression of S6K, pS6K, GLI2 and GAPDH in normal and gastric cancer patient tissues. **(K)**

Densitometric analysis of Western blots. *$p<0.05$ compared to normal, n = 6 normal and n = 50 gastric cancer patients.

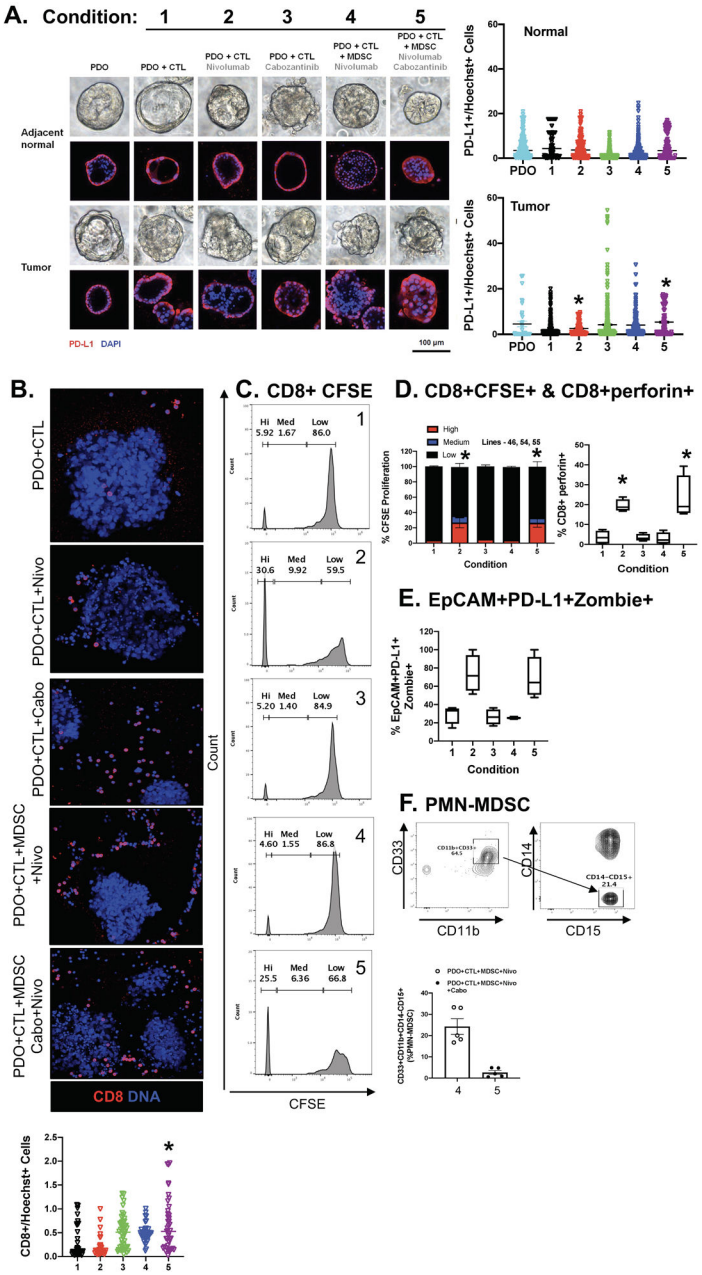

Figure 2: Effect of PMN-MDSCs in PD-L1+ PDO/immune cell co-cultures treated with nivolumab.

(**A**) Morphological changes in PDOs after 48 hours of *in vitro* treatment with vehicle (Control) alone, vehicle (Control) in co-cultures with CTLs (Condition 1), nivolumab (0.5 μg/ml; Condition 2) or Cabozantinib (10 μM; Condition 3) in co-cultures with CTLs, nivolumab (Condition 4) or a combination of nivolumab and Cabozantinib (Condition 5) in co-cultures with CTLs and MDSCs. (**B**) Images showing changes in organoid viability and CD8+ cell expression in organoid co-cultures. **(C)** Measurement of changes in CTL proliferation by CFSE, with quantification shown in **(D)**. Changes in **(D)** perforin expression in CTLs, **(E)** percent of viable EpCAM+/PD-L1+ organoids and **(F)** PMN-MDSCs in

response to treatments. *p<0.05 compared to condition 1, n = 4 organoid co-cultures derived from individual patients.

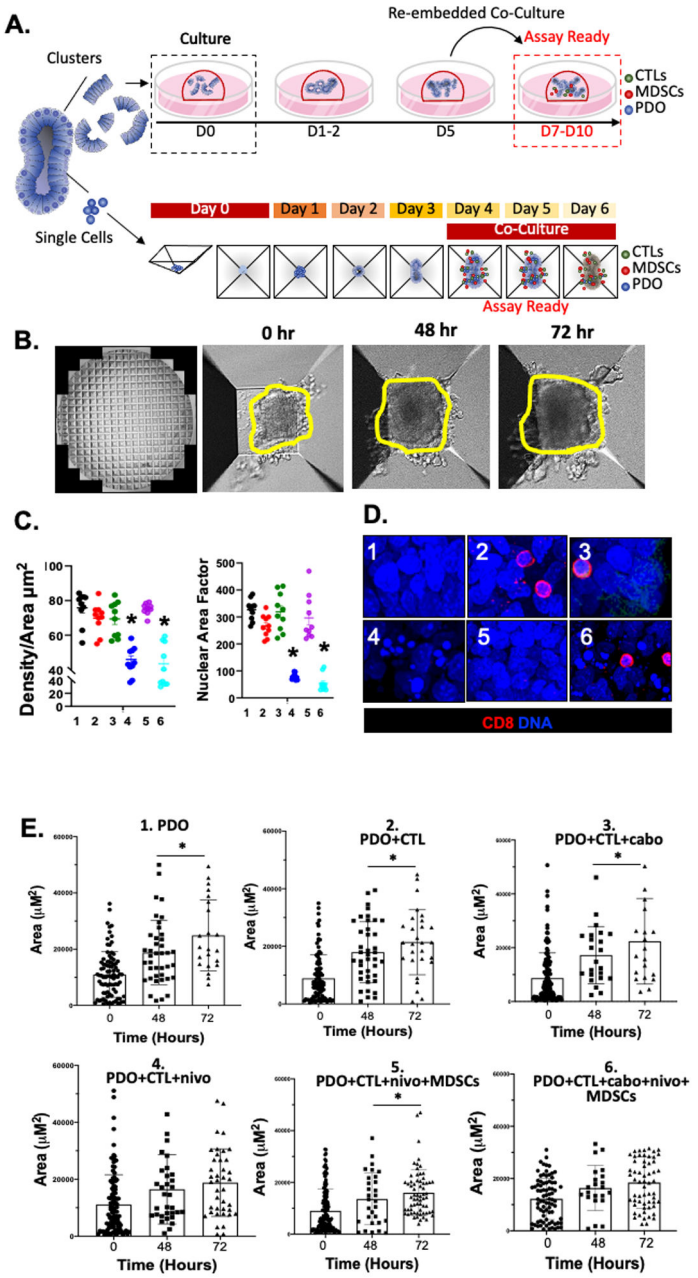

Figure 3: Morphological changes in PD-L1+ PDO/immune cell co-cultures in response to nivolumab.

(**A**) Schematic diagram showing the generation and timeline of organoid/immune cell co-culture using either Matrigel® dome or AggreWell™ microwell plates. **(B)** Representative images of morphological changes of PDO/immune cell co-cultures after 0, 48 and 72 hours of treatment in AggreWell™ microplates (yellow outlining indicates increased organoid area. **(C)** Changes in Density/Area (μm^2) and nuclear area factor 72 hours after treatment in conditions 1 - 6. **(D)** Immunofluorescence showing expression of CD8+ cells (red) and nuclei stained by DAPI 72 hours after treatment in conditions 1 – 6. **(E)** Change in organoid Area ((μm^2) in vehicle (condition 1) in co-cultures with CTLs (condition 2), cabozantinib

(condition 3) or nivolumab (condition 4) in co-cultures with CTLs, nivolumab (condition 5) or a combination of nivolumab and cabozantinib (condition 6) in co-cultures with CTLs and MDSCs at 0, 48 and 72 hours. *$p<0.05$ compared to 0hr/vehicle treated for each condition besides condition 4 and 6 (ns= nonsignificant), n = 4 organoid co-cultures derived from individual patients.

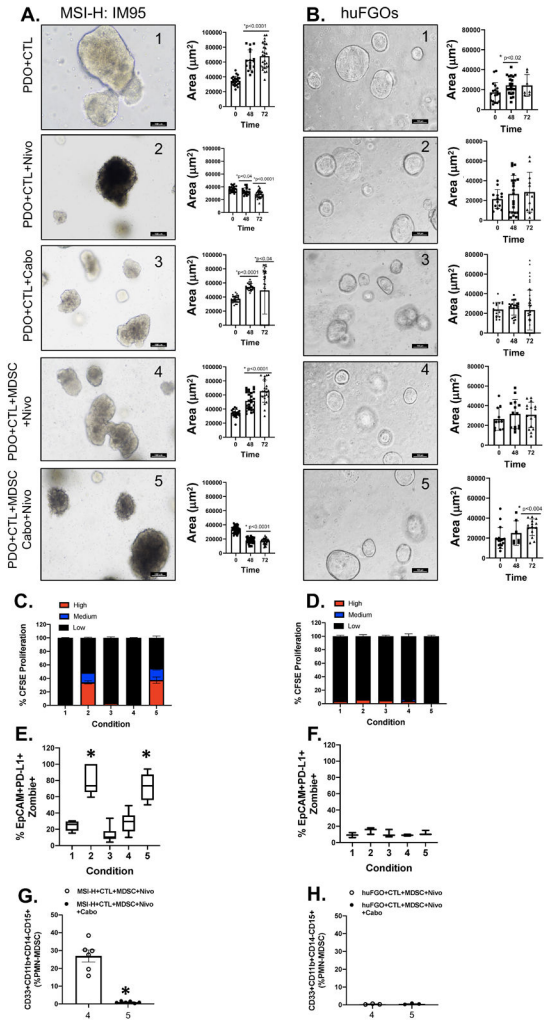

Figure 4: Effect of PMN-MDSCs on CTL proliferation and cancer cell death in PD-L1+ PDO/immune cell co-cultures.

Changes in morphology and Area (μm^2) of (**A**) MSI-H IM95 gastric cancer/immune cell co-cultures, and (**B**) huFGO/immune cell co-cultures after 48 and 72 hours of *in vitro* treatment with vehicle in co-cultures with CTLs (condition 1), nivolumab (condition 2) or cabozantinib (condition 3) in co-cultures with CTLs, nivolumab (condition 4) or a combination of nivolumab and cabozantinib (condition 5) in co-cultures with CTLs and MDSCs. (**C**) CTL proliferation, (**E**) organoid viability, and (**G**) PMN-MDSC numbers were quantified by flow cytometry in MSI-H IM95 organoid/immune cell co-cultures. (**D**) CTL proliferation, (**F**) organoid viability, and (**H**) PMN-MDSC numbers were quantified by flow cytometry in hFGO/immune cell co-cultures. *$p<0.05$ compared to condition 1, n = 4 organoid co-cultures derived from individual patients or experimental replicates for IM95 cells.

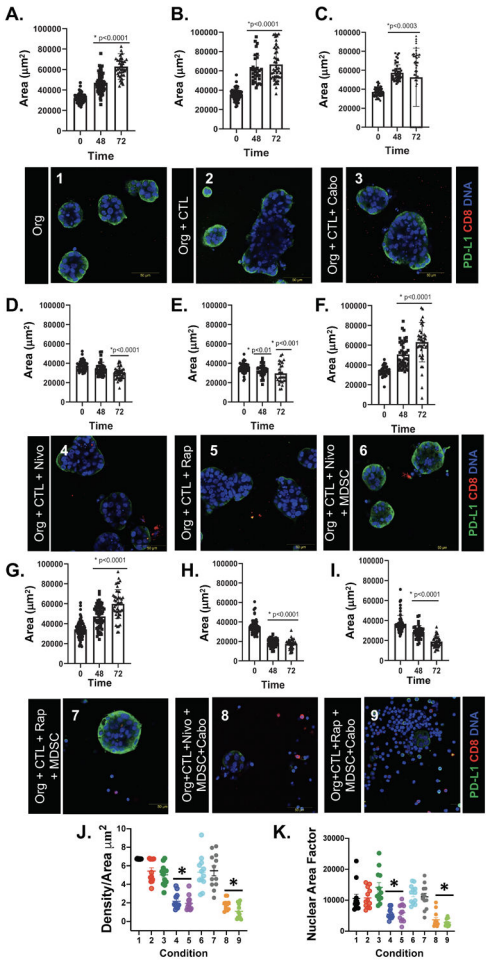

Figure 5: Morphological changes in PD-L1+ PDO/immune cell co-cultures in response to nivolumab and rapamycin treatments.

Changes in organoid area (µm^2) and PD-L1 expression by immunfluorescence in **(A)** organoids (org) treated with vehicle (condition 1), **(B)** org+CTLs (condition 2), **(C)** org+CTLs treated with cabozantinib (condition 3), or **(D)** nivolumab (condition 4), or **(E)** rapamycin (condition 5), **(F)** org+CTLs+MDSCs treated with nivolumab (condition 6) or **(G)** rapamycin (condition 7), **(H)** org+CTLs+MDSCs treated with nivolumab plus cabozantinib condition 8), and **(I)** org+CTLs+MDSCs treated with rapamycin plus cabozantinib (condition 9). Morphological changes in co-cultures were quantitatively analyzed by measuring changes in **(J)** density/area (µm^2), and **(K)** nuclear area factor. *p<0.05 compared to 0hr for each condition, n = 4 organoid co-cultures derived from individual patients.

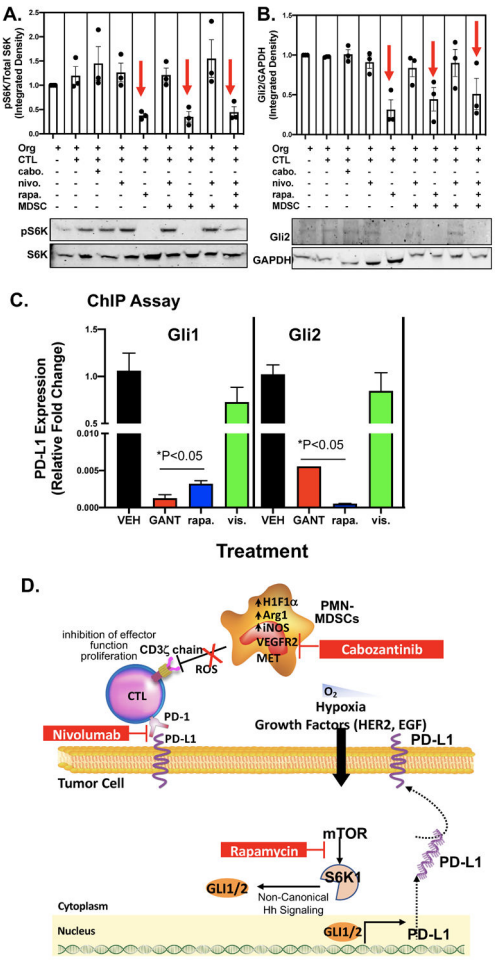

Figure 6: Effect of rapamycin on GLI expression and transcriptional regulation of PD-L1.

Protein extracted from MSI-H cell-derived organoid/immune cell co-cultures were used in western blots measuring changes in **(A)** phosphorylated S6K (phosphor-S6K) and total S6K, and **(B)** Gli2 and GAPDH expression. **(C)** ChIP assay was used to measure the transcriptional regulation of PD-L1 by Gli1 and Gli2 in response to co-cultures treated with vehicle (VEH), rapamycin (rapa.), GANT61 or vismodegib (vis.). *p<0.05 compared to organoids alone, n = 4 experimental replicates. **(D)** Proposed mechanism regulating PD-L1 expression in gastric cancer cells. Within the gastric tumor microenvironment, PMN-MDSCs override the effectiveness of checkpoint inhibition by producing Arg1, iNOS and ROS. Pharmacological inhibition of PMN-MDSCs may deplete the cells from the tumor microenvironment and sensitize patients to immunotherapy. Hh-induced PD-L1 expression is mediated by the mTOR signaling pathway.